




Lack of compensatory mitophagy in skeletal muscles during sepsis

Sami Sedraoui^{1,2}, Jean-Philippe Leduc-Gaudet³ , Dominique Mayaki^{1,2}, Alaa Moamer^{1,2}, Laurent Huck^{1,2}, Gilles Gouspillou⁴ , Basil J. Petrof^{1,2}  and Sabah Hussain^{1,2,5} 

¹Meakins-Christie Laboratories, Department of Medicine, McGill University, Montreal, QC, Canada

²Translational Research in Respiratory Diseases Program, Research Institute of the McGill University Health Centre, Montreal, QC, Canada

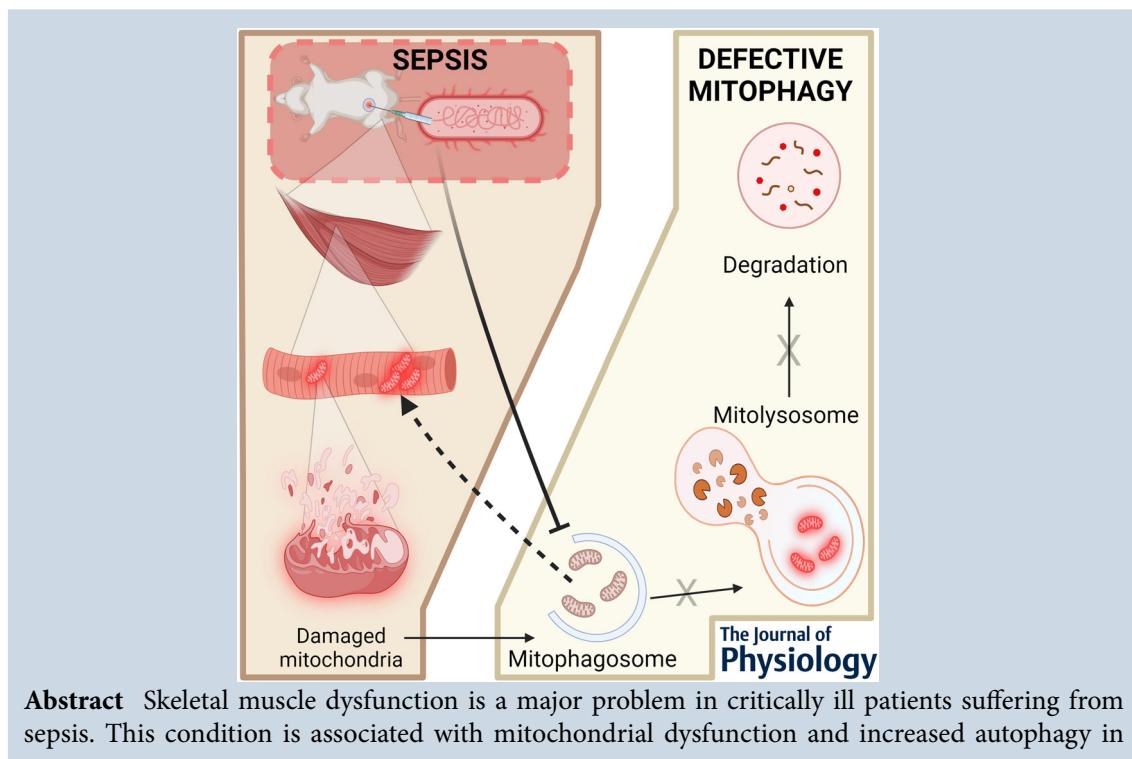
³Department of Medical Biology, Faculty of Health Sciences, Université du Québec à Trois-Rivières, Trois-Rivières, QC, Canada

⁴Département des Sciences de l'Activité Physique, Faculté des Sciences, Université du Québec à Montréal, Montréal, QC, Canada

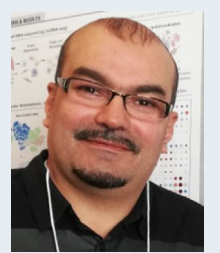
⁵Department of Critical Care Medicine, McGill University Health Centre, Montreal, QC, Canada

Handling Editors: Karyn Hamilton & Matthew Brook

The peer review history is available in the Supporting Information section of this article (<https://doi.org/10.1113/JP286216#support-information-section>).



Sami Sedraoui obtained his PhD at University of Carthage, Tunisia, under the supervision of Professor Zouhair Tabka and co-supervision of Professor Yves Desjardins at University Laval, Quebec, Canada. His PhD project focused on the optimization of the extraction of antioxidants compounds from palm date fruit (*Phoenix dactylifera* L.) and their effect on skeletal muscle atrophy and autophagy. Sami joined the Meakins-Christie laboratories at McGill University in Montreal, Canada in 2022 as a postdoctoral fellow under the supervision of Professor Sabah NA Hussain. His research investigates skeletal muscle mitophagy regulation and monitoring under normal and catabolic conditions.



B. J. Petrof and S. Hussain contributed equally to this work.

skeletal muscles. Autophagy is a proteolytic mechanism involved in eliminating dysfunctional cellular components, including mitochondria. The latter process, referred to as mitophagy, is essential for maintaining mitochondrial quality and skeletal muscle health. Recently, a fluorescent reporter system called mito-QC (i.e. mitochondrial quality control) was developed to specifically quantify mitophagy levels. In the present study, we used mito-QC transgenic mice and confocal microscopy to morphologically monitor mitophagy levels during sepsis. To induce sepsis, Mito-QC mice received *Escherichia coli* lipopolysaccharide (10 mg kg⁻¹ I.P.) or phosphate-buffered saline and skeletal muscles (hindlimb and diaphragm) were excised 48 h later. In control groups, there was a negative correlation between the basal mitophagy level and overall muscle mitochondrial content. Sepsis increased general autophagy in both limb muscles and diaphragm but had no effect on mitophagy levels. Sepsis was associated with a downregulation of certain mitophagy receptors (Fundc1, Bcl2L13, Fkbp8 and Phbb2). The present study suggests that general autophagy and mitophagy can be dissociated from one another, and that the characteristic accumulation of damaged mitochondria in skeletal muscles under the condition of sepsis may reflect a failure of adequate compensatory mitophagy.

(Received 2 January 2024; accepted after revision 2 May 2024; first published online 15 May 2024)

Corresponding author S. Hussain: Room EM2.2224, 1001 Decarie Blvd, Montreal, Montreal, Quebec H4A 3J1, Canada.
Email: sabah.hussain@muhc.mcgill.ca

Abstract figure legend The defective mitophagy pathway under sepsis is explained by inhibition (continuous line) of the engulfment of damaged mitochondria by autophagosomes to form mitophagosomes leading to the accumulation of damaged mitochondria within skeletal muscle fibres (dashed line).

Key points

- There was a negative correlation between the basal level of skeletal muscle mitophagy and the mitochondrial content of individual muscles.
- Mitophagy levels in limb muscles and the diaphragm were unaffected by lipopolysaccharide (LPS)-induced sepsis.
- With the exception of BNIP3 in sepsis, LPS administration induced either no change or a down-regulation of mitophagy receptors in skeletal muscles.

Introduction

Skeletal muscle weakness in critically ill patients, referred to as intensive care unit-acquired muscle weakness, is associated with an increased risk of prolonged hospitalization and death (Fan et al., 2014). It can involve both limb muscles and the diaphragm and is frequently observed in patients with severe sepsis. Sepsis is associated with abnormal morphological and functional abnormalities within skeletal muscle fibres, such as signs of skeletal muscle atrophy and injury (Petrof, 2018). In addition, it has been shown that sepsis induces mitochondrial dysfunction in skeletal muscles, strongly correlating with atrophy and contractile abnormalities. Skeletal muscles affected by sepsis exhibit notable ultrastructural abnormalities in mitochondria, including extensive swelling, disrupted cristae and damaged matrices (Mofarrahi et al., 2012).

Mitochondria represent dynamic networks that continually adjust to the cellular demands of their resident tissue. The morphology and function of mitochondria hinge on a delicate equilibrium between fusion and fission processes. Fusion facilitates the creation of an expansive interconnected network, promoting the intermingling of their contents within this network. Conversely, fission serves to segregate malfunctioning mitochondria from the larger network, allowing for their subsequent elimination and recycling through a form of autophagy that is selective for mitochondria, known as mitophagy (Leduc-Gaudet et al., 2021). Autophagy is typified by the generation of double-membrane vesicles, termed autophagosomes, which envelop organelles (such as mitochondria, peroxisomes and endoplasmic reticulum), cytosolic components and protein aggregates. These autophagosomes transport their cargo to lysosomes for degradation (Klionsky, 2008). Previous work by

ourselves and other groups has demonstrated that general autophagy is induced in skeletal muscles by sepsis, although the specific impact of this catabolic conditions on mitophagy is unknown (Stana et al. 2017; Mofarrahi et al. 2013).

Different methods and approaches are available for quantifying mitophagy. The most direct but resource-intensive method involves transmission electron microscopy, where the quantification of autophagosomes containing mitochondria occurs, albeit at a high cost in terms of both time and expertise (Duan et al., 2022). An alternative approach utilizes immunofluorescence staining, where lysosomal-specific staining is co-localized with fluorescent mitochondrial markers. However, a significant limitation of this method is the potential proximity of mitochondria to lysosomes without undergoing degradation by these organelles (Montava-Garriga et al., 2020). A more recent development in mitophagy quantification involves the use of a transgenic mouse model called mito-QC (i.e. mitochondrial quality control), designed to assess mitophagy under *in vivo* conditions (McWilliams et al., 2016). This model incorporates a tandem-fusion protein that expresses mCherry and green fluorescence protein (GFP) fused to a segment of the FIS1 protein (a mitochondrial outer membrane protein). The fusion protein enables the quantification of mitophagy by detecting an increase in the red (mCherry) fluorescence signal when the GFP signal is quenched upon the delivery of mitochondria to the lysosomes (an acidic environment) (McWilliams & Ganley, 2019). Recent studies have employed the mito-QC reporter mouse model to quantify mitophagy in various organs, including skeletal muscles (Goljanek-Whysall et al., 2020; Mito et al., 2022).

In the present study, we hypothesized that the accumulation of morphologically and functionally deranged mitochondria in limb and diaphragm skeletal muscles during sepsis could reflect a relative failure of autophagy to clear these abnormal mitochondria. This would imply that, despite the known increase in general autophagy under this condition (Azuelos et al., 2015; Mofarrahi et al., 2012), there is an inadequate level of mitophagy. Therefore, the primary objective of our study was to quantify mitophagy in both limb muscles and the diaphragm in response to sepsis using the newly developed mito-QC reporter mouse system.

Methods

Ethical approval

The present study was carried out in strict accordance with standards established by the Canadian Council of Animal Care and the guidelines and policies of McGill University. All procedures were approved by

the Animal Ethics Committees of McGill University ((#2022-7549). Experimental protocols were designed to minimize suffering and the number of animals used in the study.

Stimulation of mitophagy in myotubes. Primary satellite cells were isolated from the diaphragm of 6-week-old male mito-QC mouse by magnetic bead separation, using a commercially available kit (Satellite Cell Isolation Kit, #130-104-268; Miltenyi Biotec, Auburn, CA, USA) in accordance with the manufacturer's instructions. The derived satellite cells were transformed into myoblasts by culturing them in a growth medium composed of 10% fetal bovine serum and a 1:1 ratio of Dulbecco's modified Eagle's medium (DMEM) + Glutamax (#31765; Gibco, Waltham, MA, USA) and F12 + Glutamax (#31966; Gibco) at 37°C and 5% CO₂. Subsequently, myoblasts were differentiated into myotubes by transitioning to a differentiation medium (DMEM supplemented with 2% heat-inactivated horse serum) for a duration of 5 days. To induce mitophagy, myotubes were exposed to the mitochondrial uncoupler carbonyl cyanide p-trichloromethoxyphenyl hydrazone (CCCP) at concentrations of 10 and 50 μM for 12 h. Control myotubes were treated with the same quantity of vehicle (DMSO). Following the treatment, cells were washed twice with sterile phosphate-buffered saline (PBS), fixed with 3.7% paraformaldehyde (#P6148; Sigma-Aldrich, St Louis, MO, USA) for 10 min and subsequently imaged using a confocal microscope (LSM 780; Zeiss, Oberkochen, Germany).

Mito-QC *in vivo* model

Animal procedures. All experimental protocols were approved (#2022-7549) by the Animal Use and Ethics Committee of the Research Institute of the McGill University Health Centre (MUHC-RI). The experiments were conducted in accordance with the principles outlined by the Canadian Council of Animal Care and the ARRIVE guidelines. Female and male homozygous C57BL/6J mito-QC (mCherry-GFP-Fis1¹⁰¹⁻¹⁵²) reporter mice were generated as previously described (McWilliams et al., 2016) and used for all *in vivo* experiments. All mice were group-housed under a standard 12:12 h light/dark photoperiod with food and water available *ad libitum*.

Stimulation of mitophagy *in vivo*. To induce mitophagy in limb muscles, adult homozygous C57BL/6J mito-QC (mCherry-GFP-Fis1¹⁰¹⁻¹⁵²) reporter mice (16 weeks old, *n* = 4, males) were group-housed under a standard 12:12 h light/dark photoperiod with food and water available *ad libitum*. Mice were anaesthetized with 2.5% to 3.5% isoflurane balanced with O₂. Adequacy of the depth of

anaesthesia was assessed by monitoring muscle reflex, rate of respiration and nose colour. Subsequently, CCCP (2.5 mg kg^{-1}) was i.m. injected into the tibialis anterior (TA) muscle of the left leg, whereas the contralateral TA muscle, serving as the control, was injected with the same quantity of vehicle (DMSO). Some 12 h later, mice were killed with 5% isoflurane balanced with O_2 , followed by cervical dislocation. Muscles were swiftly excised and prepared for histology using established procedures (Leduc-Gaudet et al., 2020).

Sepsis. To simulate human acute sepsis, adult homozygous C57BL/6J mito-QC (mCherry-GFP-Fis1^{101–152}) reporter mice (48–52 weeks old, $n = 7$, males) received i.p. injections with a single dose of *Escherichia coli* lipopolysaccharide (LPS) (10 mg kg^{-1} i.p., serotype 055: B5; Sigma-Aldrich). Control mice (48–52 weeks old, $n = 7$, males) received the same i.p. volume of PBS. Throughout the first 12 h following LPS injection, and thereafter every 12 h, animals were observed for clinical signs such as diarrhoea, decreased mobility, hunched posture, ruffled fur and weight loss. Any animals experiencing weight loss exceeding 20% or showing a respiratory quality score greater than 3 within 48 h of LPS injection were killed under isoflurane anaesthesia and subsequently excluded from the study. Otherwise, both control and LPS-treated animals were killed under isoflurane anaesthesia followed by cervical dislocation, as described above. TA, soleus (SOL) and diaphragm (DIA) muscles were promptly excised and divided into two portions. The first portion underwent histological preparation for mito-QC analysis by confocal microscopy following the procedures outlined originally (McWilliams & Ganley, 2019). The second portion of the muscle was rapidly frozen in liquid nitrogen and stored at -80°C for subsequent analysis.

Confocal microscopy. Freshly excised muscles were fixed overnight by immersion into a freshly prepared 3.7% paraformaldehyde in 200 mM HEPES (pH 7.0). Tissues were cryoprotected in a sucrose 30% (w/v) solution containing 0.04% sodium azide. Samples were then mounted and frozen sectioned with a cryostat (CM1860UV; Leica). Eight-micron sections were placed on slides and mounted using Vectashield Antifade Mounting Medium (H-1000; Vector Laboratories, Newark CA, USA). Mito-QC myotubes and muscle sections were imaged using laser-scanning confocal microscopy (LSM 780; Zeiss). Confocal pictures were obtained by uniform random sampling using the optimal parameters for acquisition.

Mitophagy quantification was conducted using the mito-QC counter macro in FIJI, version 1.52n (ImageJ; NIH, Bethesda, MD, USA), as previously outlined

(Montava-Garriga et al., 2020). In brief, seven $10\times$ random mito-QC-myotube images for each condition and ten $63\times$ random mito-QC muscle section images per sample were analysed using the mito-QC counter macro, with each image defined as a region of interest. The macro generates a new image from the original by calculating the ratio between the intensity of each pixel in the mCherry 'red' channel and the equivalent in the GFP 'green' channel. Regions with high mCherry/GFP intensity ratios are identified as red puncta, indicative of mitolysosomes. The macro detects these puncta as peaks, applying a filter to eliminate background noise. Subsequently, a threshold is set on the ratio image to exclude pixels where the red channel intensity falls below the threshold value, and peaks are then counted and quantified as the number of mitolysosomes. In accordance with the original methodology (Montava-Garriga et al., 2020), the intensity of the reporter in the green channel per tissue area reflects the amount of muscle mitochondria. This measurement serves as a readout for mitochondrial content to evaluate the proportional expression of the mito-QC reporter relative to muscle oxidative metabolism.

Immunoblotting. Approximately 20 mg of muscle sample were homogenized in an ice-cold lysis buffer (50 mM HEPES, 150 mM NaCl, 100 mM NaF, 5 mM EDTA, 0.5% Triton X-100, 0.1 mM DDT, $2 \mu\text{g mL}^{-1}$ leupeptin, $100 \mu\text{g mL}^{-1}$ phenylmethylsulfonyl fluoride, $2 \mu\text{g mL}^{-1}$ aprotinin and 1 mg per 100 mL of pepstatin A, pH 7.2) using Mini-bead beater (BioSpec Products) with a ceramic bead at 60 Hz. Muscle homogenates were then centrifuged at 5000 g for 15 min at 4°C and the supernatants were collected. After protein content measurement using the Bradford assay, aliquots of crude muscle homogenates were mixed with Laemmli buffer (6 \times , reducing buffer; #BP111R; Boston BioProducts, Ashland, MA, USA) and subsequently denatured for 5 min at 95°C . Then, $20 \mu\text{g}$ of protein extracts per lane were separated by SDS-PAGE and transferred onto polyvinylidene difluoride (PVDF) membranes (Bio-Rad Laboratories, Saint-Laurent, QC, Canada). After detecting total proteins on the membranes by using Stain-Free-Blot (SFB) technology (Bio-Rad Laboratories), PVDF membranes were blocked in PBS + 0.1% Tween[®] 20 + 5% bovine serum albumin for 1 h at room temperature and then incubated with LC3 primary antibody (dilution 1:1000; #12741; Cell Signaling Technology, Danvers, MA, USA) overnight at 4°C . After three 5 min washes, membranes were incubated with horseradish peroxidase-conjugated secondary anti-rabbit antibody (catalog. no. Ab6728; Abcam; Toronto, ON, Canada) for 1 h at room temperature, before further washing in PBS-Tween 20 ($3 \times 5 \text{ min}$). Immunoreactivity was detected using an enhanced chemiluminescence substrate (Pierce[™], Thermo Fisher Scientific, Saint-Laurent,

Table 1. List of qPCR primers

Gene	Accession number	Forward primer (5'- to 3')	Reverse primer (5'- to 3')
Pgk1	NM_0 08828	CAAGGCTTTGGAGAGTCCAG	TGTGCCAATCTCCATGTTGT
Cyclophillin	AY427600	GCATCTTCTTCGAGCTGTT	CTGGACATGAATCCTGGAA
Atrogin	NM_02 6346	TGGGTGTATCGGATGGAGAC	TCAGCCTCTGCATGATGTTC
MuRF1	NM_0 010 39048	TGCTTGGCACTTGAGAGGAA	AGAAGCTGGGCTTCATCGAG
Map1lc3b	NM_02 6160	CGATACAAGGGGGAGAAGCA	ACTTCGGAGATGGGAGTGGGA
Gabarp1	NM_02 0590.4	GAGGACCACCCCTTCG	CGGAGGGCACAAGGTACTTC
Beclin1	NM_01 9584	CTTGGAGGAGGAGGCTGA	TGTGGAAGGTGGCATTGAAG
Bnip3	NM_0 09760	ACCAGGAAATGAGCTTGACAA	ACCAGGAAATGAGCTTGACAA
Bnip3L	XM_01 822 5163	TTGGGGCATTCTTAACCTTG	TGCAGGTGACTGGTGGTACTAA
Parkin	NM_01 6694	TCTTCCAGTGTAACCACCGTC	GGCAGGGAGTAGCCAAGTT
Fundc1	NM_02 8058	CCCCTCCCCAAGACTATGAA	CGCCACCCATTACAATCTGA
Ndp52	NM_0 012 71018	CCACACAGCAGGAAATCCAA	TCGTCAGGGTCTGGACAAAA
Optn	NM_0 013 56487	TATCCAGAGCCTTGAGGGA	AGCAGGTCTGCCTTTTCAG
Bcl2l13	XM_0 065 06814	CAGATTGCAATGGACCTGA	CACGGTAGGGACCTGTGTGA
Fkbp8	NM_0 011 11066	CATGGTTACCGCTGACTCCA	CCGTCTCAGGGTGACTTCC
Phb2	NM_0 07531	ATGGCCCAGAACTGAAGGA	GCTCTATGACCGCCTTCCAC
Rab7	NM_0 07531	CTCGACAGCTGGAGAGACGA	TGCTGTAGCACCAGCCTGT
TNF- α	NM_01 3693	ACTGGCAGAAGAGGCACTCC	CTCCAGCTGCTCCTCACTT
IL-6	NM_03 1168	CACGGCCTTCCCTACTTAC	TGCAAGTGATCATCGTTGT
IL-1 β	NM_0 08361	GTGGCTGTGGAGAAGCTGTG	CGGAGCCTGTAGTGACAGTTG

QC, Canada) with the ChemiDoc™ XRS+ Imaging System. The optical densities of the protein bands were quantified using ImageLab (Bio-Rad Laboratories) and normalized to loading control (SFB-PVDF membranes).

Transmission electron microscopy (TEM). Samples for TEM were prepared as previously described (Picard et al., 2013). Briefly, small strips of muscle prepared from TA, SOL and DIA of control and LPS-injected mito-QC mice were incubated in 2% glutaraldehyde buffer solution in 0.1 M cacodylate (pH 7.4) and subsequently post-fixed in 1% osmium tetroxide in 0.1 M cacodylate buffer. Tissues were then dehydrated via increasing concentrations of methanol to propylene oxide and infiltrated and embedded in epoxy resin (Epon) blocks at the Facility of Electron Microscopy Research of McGill University. Ultrathin sections (60 nm) were cut in the longitudinal plane using an ultramicrotome (Ultracut III; Reichert-Jung, Munich, Germany) and mounted on nickel carbon-formvar coated grids for electron microscopy. Uranyl acetate and lead citrate-stained sections were then imaged using Tecnai 12 transmission electron microscope (FEI, Hillsboro, OR, USA) at 120 kV and images were digitally captured using a XR80C CCD camera system (Advanced Microscopy Techniques, Woburn, MA, USA) at a magnification of 1400 \times .

Quantitative real-time PCR (qRTR-PCR). Total RNA was extracted from frozen muscle samples using a PureLink™ RNA Mini Kit (Invitrogen Canada, Burlington, ON,

Canada). Quantification and purity of RNA was assessed using the A_{260}/A_{280} absorption method (A_{260}/A_{280} ratio between 1.8 and 2). Total RNA (2 μ g) was reverse transcribed using a Superscript II® Reverse Transcriptase Kit and random primers (Invitrogen Canada). Reactions were incubated at 42°C for 50 min and at 90°C for 5 min. RT-PCR detection of mRNA expression was performed using a Prism® 7000 Sequence Detection System (Applied Biosystems, Foster City, CA, USA). Cycle threshold (C_T) values were obtained for each target gene. ΔC_T values (normalized gene expression) were calculated as C_T of target gene minus C_T of the geometric means of two housekeeping genes (*Cyclophilin B*, *Pgk1*). Relative mRNA level quantifications of target genes were determined using the threshold cycle ($\Delta\Delta C_T$) method. The primer sequences for all genes are provided in Table 1.

Statistical analysis. All statistical analyses were conducted using Prism, version 8 (GraphPad Software Inc., San Diego, CA, USA). For the *in vivo* CCCP and sepsis experiments, variables were compared using unpaired *t* tests. In the case of *in vitro* CCCP experiments and basal mitophagy comparison between different skeletal muscles in control mice, one-way analysis of variance (ANOVA) was utilized if there were no missing values; otherwise, mixed-effects analysis was employed. Corrections for multiple comparisons following ANOVA or mixed-effects analysis were carried out by controlling for the false discovery rate using the two-stage step-up method of Benjamini, Krieger and Yekutieli. $P < 0.05$ and

$q < 0.1$ were considered statistically significant. The exact number of animals is indicated where appropriate, and all data in bar graphs are presented as the mean \pm SD.

Results

Stimulation of mitophagy in myotubes

To induce mitophagy *in vitro*, we subjected primary mito-QC myotubes to a 12 h exposure to the mitochondrial uncoupler CCCP, which is known to decrease mitochondrial membrane potential that leads to induction of mitophagy. The myotubes exhibited a noticeable reduction in abundance, a slenderer morphology and diminished GFP fluorescence intensity (indicator of mitochondrial content) compared to control

myotubes (Fig. 1). Furthermore, exposure to CCCP at concentrations of 10 and 50 μM led to a 25% increase in the number of mitolysosomes (red punctae) normalized to surface area and a two- to three-fold rise in the number of mitolysosomes normalized to mitochondrial content, respectively (Fig. 1).

Stimulation of mitophagy in intact muscles

We administered CCCP (2.5 mg kg^{-1} i.m.) into the TA muscle *in vivo* and removed the muscles 12 h later. Similar to the *in vitro* myotube model, CCCP injection resulted in a decrease in mean green reporter intensity and an elevation in the number of mitolysosomes, normalized for either muscle surface area or mitochondrial content

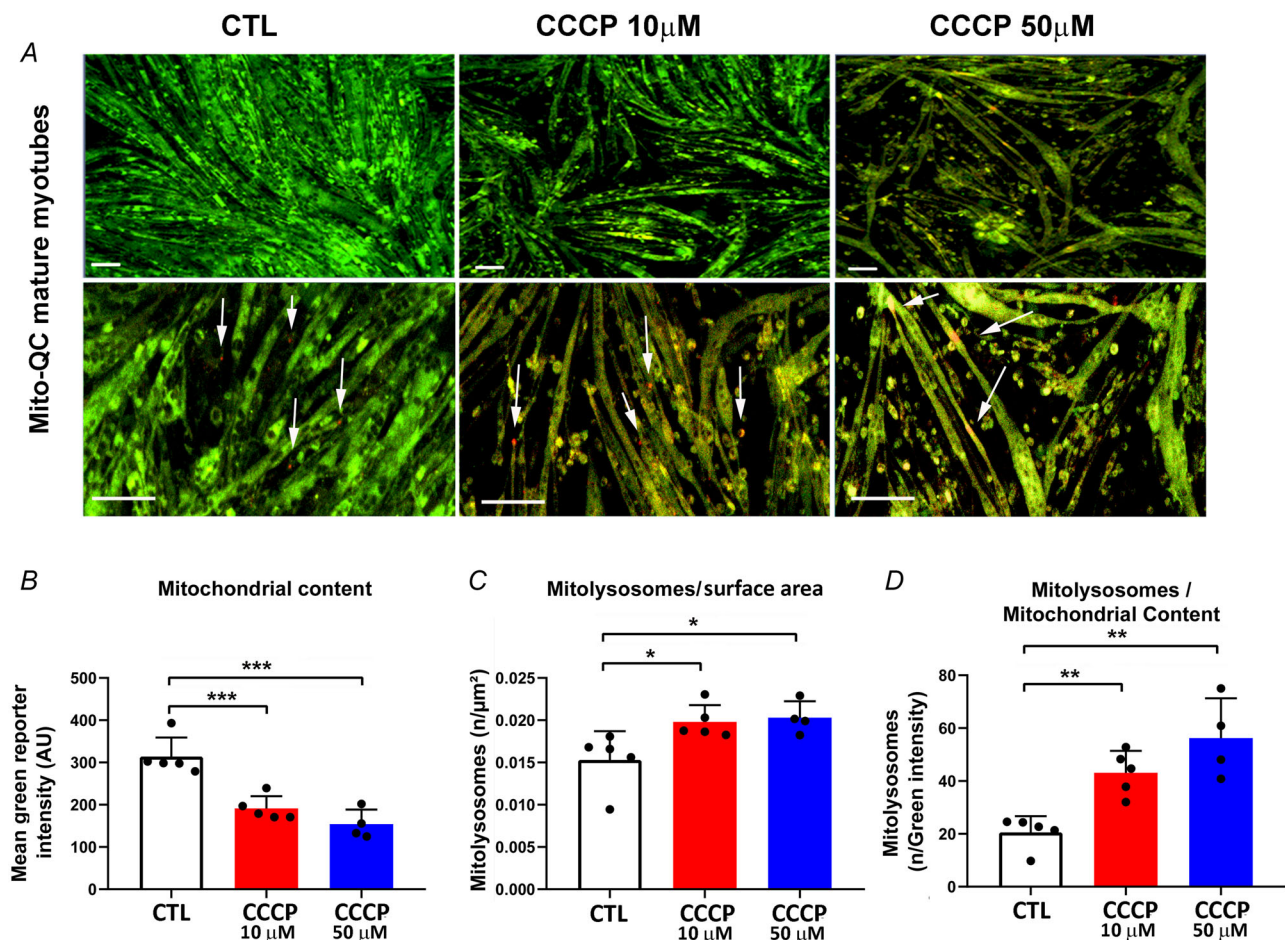


Figure 1. Stimulation of mitophagy in myotubes

A, representative confocal images of control (CTL) and CCCP-treated (12 h) differentiated primary myoblasts derived from mito-QC mouse ($n = 1$). White arrows point to mitolysosomes (red dots). White bars represent 200 μm . B–D, Mean \pm SD of green reporter intensity as an index of muscle mitochondrial content (CTL vs. CCCP 10 μM , $P = 0.0001$; CTL vs. CCCP 50 μM , $P < 0.0001$; CCCP 10 μM vs. CCCP 50 μM , $P = 0.1593$) (B), the number of mitolysosomes normalized per surface area (CTL vs. CCCP 10 μM : $P = 0.0185$; CTL vs. CCCP 50 μM , $P = 0.0146$; CCCP 10 μM vs. CCCP 50 μM , $P = 0.7750$) (C) and per mitochondrial content (CTL vs. CCCP 10 μM , $P = 0.0045$; CTL vs. CCCP 50 μM , $P = 0.0003$; CCCP 10 μM vs. CCCP 50 μM , $P = 0.0779$) (D) in control myotubes and those exposed to CCCP. Statistically significant: * $P < 0.05$, ** $P < 0.01$ and *** $P < 0.001$ compared to control myotubes.

(Fig. 2). These findings suggest that subjecting skeletal muscle mitochondria to the damaging effects of CCCP *in vivo* leads to increased mitophagy with a concurrent decrease in muscle mitochondrial content. Taken together with the *in vitro* model data, these observations confirm the ability of the mito-QC model to effectively quantify alterations in the level of mitophagy in skeletal muscle.

Basal mitophagy in skeletal muscles of control mice

To explore the relationship between basal mitophagy and the oxidative capacity of skeletal muscles in control mice, we quantified mitolysosomes and mitochondrial content in different skeletal muscles with known distinct differences in oxidative metabolism: fast-twitch muscles with high oxidative capacity (DIA), fast-twitch

muscles with low oxidative capacity [TA and gastrocnemius (GAS)] and slow-twitch muscles with high oxidative capacity (SOL). As expected, mitochondrial content (determined by GFP fluorescence intensity) was significantly higher in the DIA and SOL compared to TA and GAS of normal mice (Fig. 3A and B). By contrast, the level of mitophagy (determined by the number of mitolysosomes normalized to muscle fibre surface area or mitochondrial content) was significantly higher in the GAS and TA compared to the DIA (Fig. 3C and D). Although the number of mitolysosomes normalized to mitochondrial content in the SOL was comparable to that of GAS and TA, it was higher than that of the DIA (Fig. 3D). These results suggest an inverse relationship between oxidative capacity and basal mitophagy in skeletal muscles under normal baseline (homeostatic) conditions.

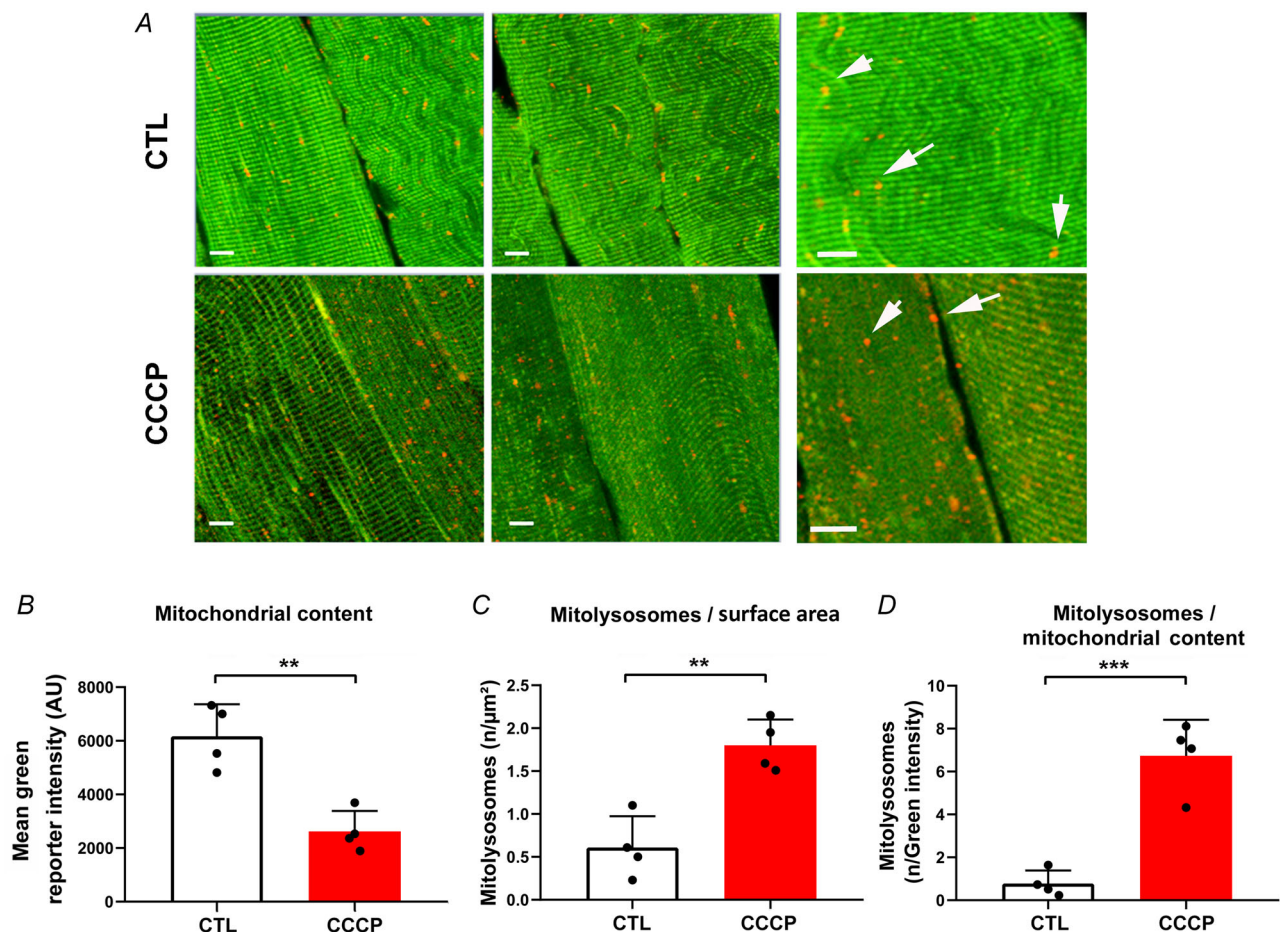


Figure 2. Stimulation of mitophagy in intact muscles

A, representative confocal images of longitudinal sections of control and CCCP-treated (12 h) TA muscle samples. White arrows point to mitolysosomes (red dots). B, Mean \pm SD of green reporter intensity of the TA of mito-QC mice as an index of muscle mitochondrial content in control TA longitudinal sections and those exposed to CCCP ($n = 4$; $P = 0.0024$). C, Mean \pm SD of number of mitolysosomes normalized per surface area in control TA longitudinal sections and those exposed to CCCP ($n = 4$; $P = 0.0024$). D, Mean \pm SD of number of mitolysosomes normalized per mitochondrial content in control TA longitudinal sections and those exposed to CCCP ($n = 4$; $P = 0.0005$). Statistically significant: $**P < 0.01$ and $***P < 0.001$ compared to control TA. White bars represent $20 \mu\text{m}$.

Impact of acute sepsis on muscle autophagy and mitophagy

It has been previously reported that sepsis activates general autophagy and proteasome proteolytic pathways in skeletal muscles (Stana et al., 2017). In the present study, we quantified markers of general autophagy consisting of Lc3b protein lipidation (by immunoblotting) and autophagy-related gene expression (by RT-PCR). Following LPS injection, the levels of the lipidated form of Lc3b (Lc3b-II) increased in the TA, SOL and DIA (Fig. 4).

The mRNA levels of Lc3b, Gabarapl1 and Beclin1 showed a pattern in which the less oxidative muscles (TA) exhibited greater upregulation of autophagy-related genes than the highly oxidative muscles (SOL and DIA) (Fig. 5). Furthermore, LPS injection substantially elevated the expression of muscle-specific

ubiquitin E3 ligases Atrogin-1 and MuRF1 in the TA, but not in the SOL (Fig. 5). In the DIA, the expression of these two E3 ligases mildly increased in response to LPS injection (Fig. 5). These findings suggest that sepsis-induced autophagy and proteasome activation are relatively more pronounced in the TA compared to the SOL and DIA.

Double-membraned autophagosomes were identified in the subsarcolemmal and intermyofibrillar regions of the TA and DIA after LPS injection (Fig. 6).

Mitochondrial contents in the TA, SOL and DIA muscles, measured by green fluorescence intensity, were not altered by LPS administration (Fig. 7A). There were no significant changes in the number of mitolysosomes in these muscles in response to LPS injection when normalized to either muscle surface area or mitochondrial content (Fig. 7B and C).

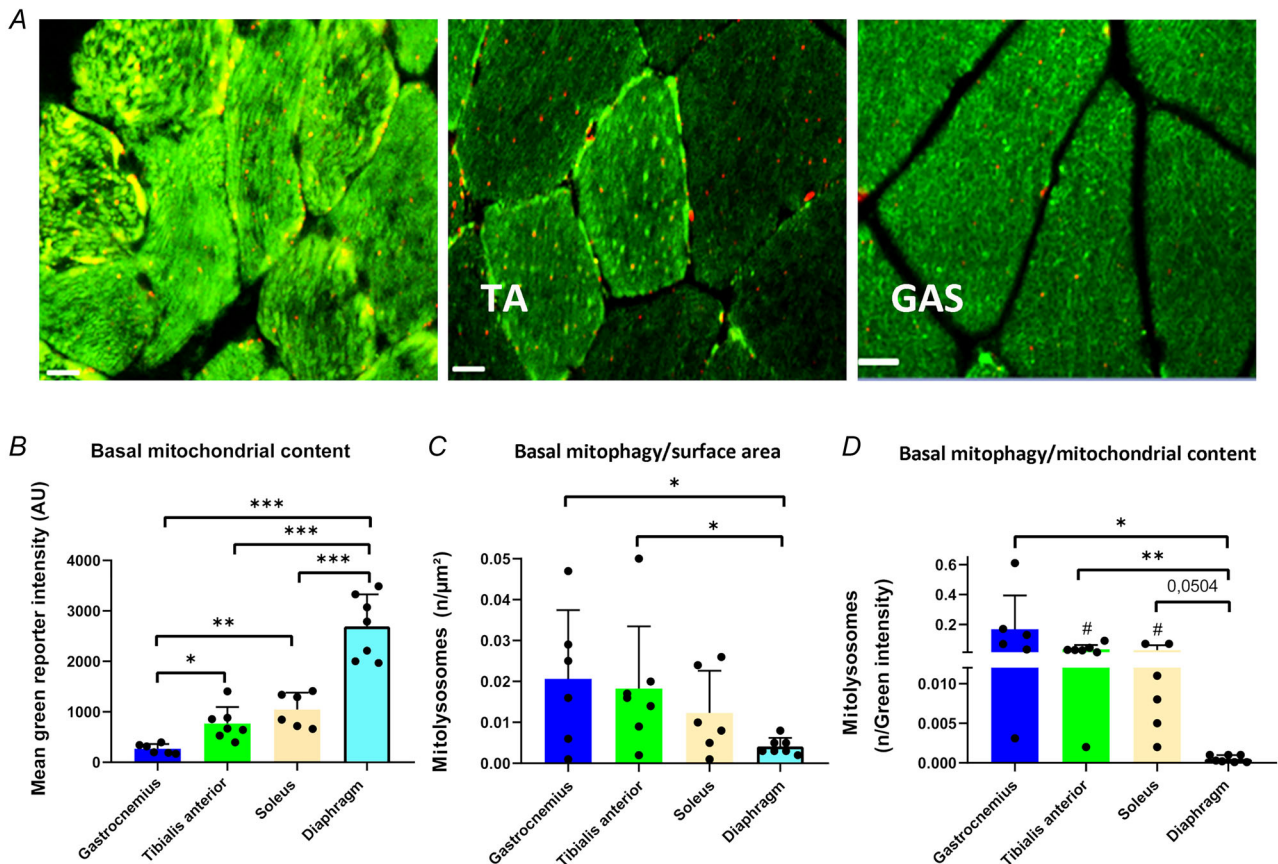


Figure 3. Basal mitophagy in limb muscles and the diaphragm in control mice

A, representative confocal images of cross-sections of DIA, TA and GAS muscles of normal mito-QC mice. Red dots indicate mitolysosomes. White bars represent 20 μm. B–D, mean ± SD of mitochondrial contents (GAS vs. TA, $P = 0.0392$; GAS vs. SOL, $P = 0.0034$; GAS vs. DIA, $P < 0.0001$; TA vs. SOL, $P = 0.2376$; TA vs. DIA, $P < 0.0001$; SOL vs. DIA, $P < 0.0001$) (B), the number of mitolysosomes normalized per muscle surface area (GAS vs. TA, $P = 0.7318$; GAS vs. SOL, $P = 0.2543$; GAS vs. DIA, $P = 0.0248$; TA vs. SOL, $P = 0.3949$; TA vs. DIA, $P = 0.0432$; SOL vs. DIA, $P = 0.2452$) (C) and per mitochondrial content (GAS vs. TA, $P = 0.0362$; GAS vs. SOL, $P = 0.0354$; GAS vs. DIA, $P = 0.0111$; TA vs. SOL, $P = 0.9253$; TA vs. DIA, $P = 0.0093$; SOL vs. DIA, $P = 0.0504$) (D) in the GAS ($n = 6$), TA ($n = 7$), SOL ($n = 6$) and the DIA ($n = 7$) of control mito-QC mice. Statistically significant: * $P < 0.05$, ** $P < 0.01$ and *** $P < 0.001$ compared to specific muscles; # $P < 0.05$ compared to GAS.

Given the lack of evidence for increased mitophagy, mRNA expression of mitophagy receptors in the TA, SOL and DIA muscles after LPS injection were also determined (Fig. 8). Bnip3 mRNA expression was increased in the three muscles in response to LPS. However, expression levels for the majority of mitophagy receptors were either

decreased or unchanged in the three muscles following LPS administration (Fig. 8).

Figure 9 illustrates the impact of LPS injection on muscle-derived pro-inflammatory cytokines including tumour necrosis alpha (TNF- α), interleukin-6 (IL-6) and interleukin-1 beta (IL-1 β). TNF- α and IL-6 mRNA

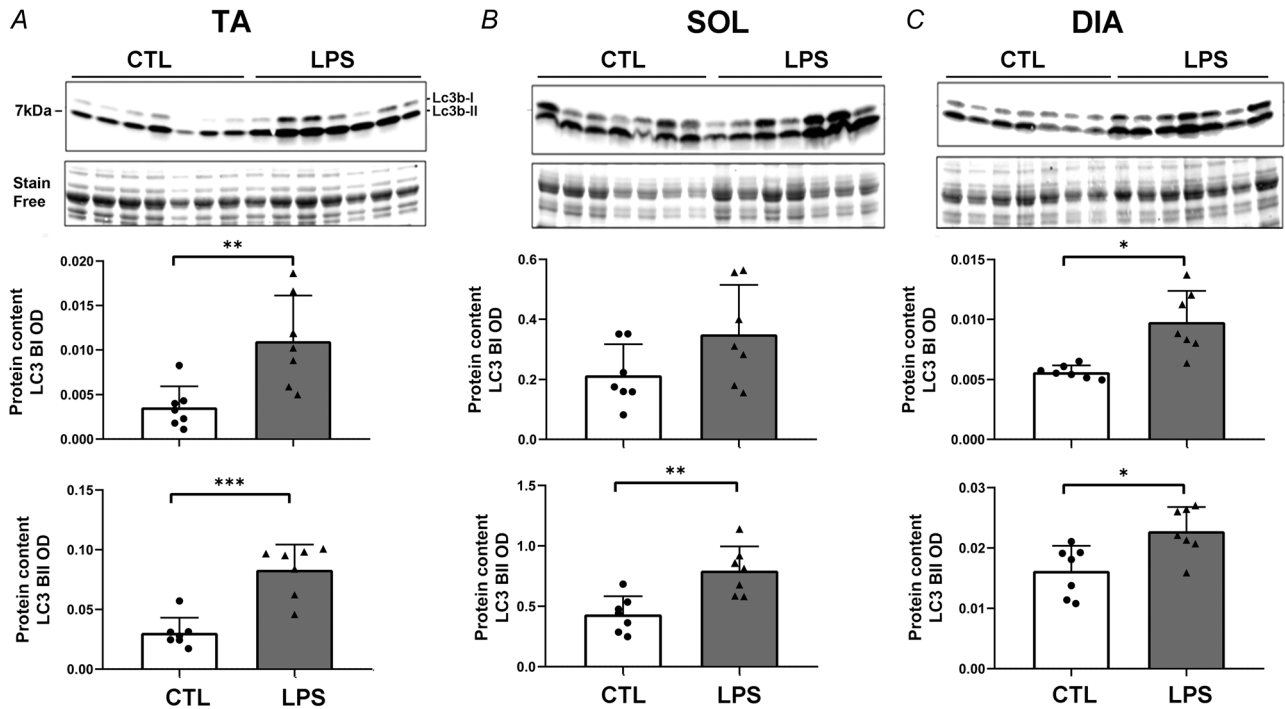


Figure 4. Impact of LPS injection on Lc3b protein expression
 Representative immunoblots and mean \pm SD of Lc3b-I and Lc3b-II protein intensities measured in the TA ($n = 7$; CTL vs. LPS for Lc3b-I, $P = 0.0046$; CTL vs. LPS for Lc3b-II, $P = 0.0001$) (A), SOL ($n = 7$; CTL vs. LPS for Lc3b-I, $P = 0.0898$; CTL vs. LPS for Lc3b-II, $P = 0.0024$) (B) and the DIA ($n = 7$; CTL vs. LPS for Lc3b-I, $P = 0.0013$; CTL vs. LPS for Lc3b-II, $P = 0.0107$) (C) of control and LPS-injected mito-QC mice. Statistically significant: * $P < 0.05$, ** $P < 0.01$ and *** $P < 0.001$ compared to control.

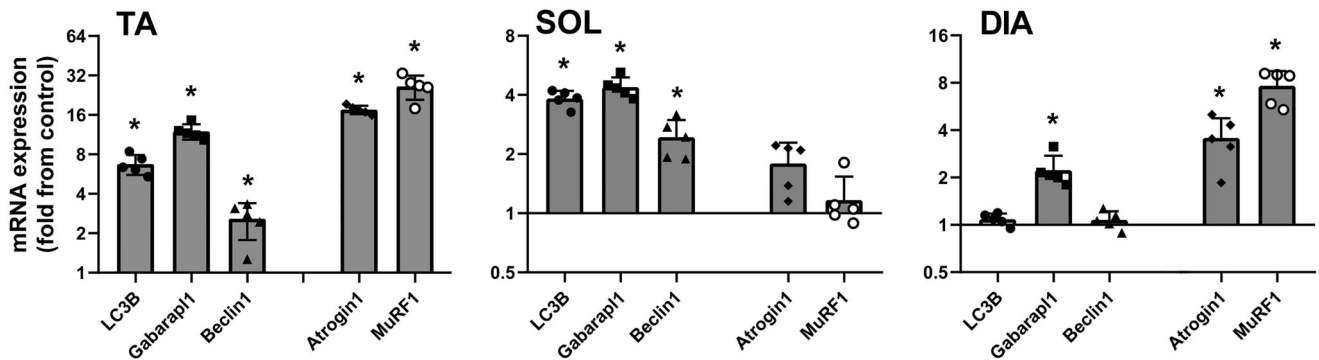


Figure 5. Impact of LPS injection on autophagy-related genes and ubiquitin E3 ligases
 Mean \pm SD of Lc3b, Gabarap1, Beclin1, Atrogin-1 and MuRF1 mRNA expression in the TA ($n = 5$; CTL vs. LPS for Lc3b, Gabarap1, Beclin1, Atrogin-1 and Murf-1, $P = 4.2887 \times 10^{-6}$; 3.26417×10^{-7} ; 0.0022 ; 5.1404×10^{-9} ; and 7.3884×10^{-6} , respectively), SOL ($n = 5$; CTL vs. LPS for Lc3b, Gabarap1, Beclin1, Atrogin-1 and Murf-1, $P = 1.3325 \times 10^{-7}$; 5.0159×10^{-7} ; 0.0003 ; 0.1604 ; and 0.9684 , respectively) and the DIA ($n = 5$; CTL vs. LPS for Lc3b, Gabarap1, Beclin1, Atrogin-1 and Murf-1, $P = 0.0886$; 0.0007 ; 0.2134 ; 0.0047 ; and 5.9385×10^{-5} , respectively) of mito-QC mice injected with LPS. Data are expressed as fold change from values measured in control mice. Statistically significant: * $P < 0.05$ compared to control.

expression increased in the TA and DIA in response to LPS, whereas IL-1 β mRNA increased only in the DIA (Fig. 9). Cytokine levels remained unchanged in the SOL muscle in response to LPS injection (Fig. 9).

Discussion

The key findings of the present study can be summarized as follows: (1) There was a negative correlation between the basal level of skeletal muscle mitophagy and the mitochondrial content of individual muscles; (2) mitophagy levels in limb muscles and the diaphragm were unaffected by LPS-induced sepsis; and (3) apart from BNIP3 during sepsis, LPS administration led to either no change or a downregulation of mitophagy receptors in skeletal muscles.

Mito-QC model of mitophagy measurements

The mito-QC model has recently been introduced as a tool to overcome limitations in measuring mitophagy in *in vivo* settings (McWilliams et al., 2016). It is based

on a pH-sensitive reporter consisting of a portion of FIS1 (mitochondrial targeting sequence) fused to GFP-mCherry proteins. When the mitochondria are delivered to the lysosomes, the GFP fluorescence is quenched because of the acidic environment, thereby leaving only mCherry fluorescence, which is then quantified as an index of mitophagy. This model has been used successfully to measure mitophagy in various murine organs in intact mice under normal and pathological conditions. To our knowledge, four published studies have so far used the mito-QC reporter to quantify mitophagy in muscle cells and intact fibres. McWilliams et al. (2016) developed a macro to quantify tissue mitophagy and reported that skeletal muscles have relatively high rate of mitophagy relative to other tissues. Mito et al. (2022) injected the mito-QC reporter construct directly into limb muscles of mice using adenoassociated virus vector and showed that accumulation of pathogenic mtDNA variants in adult-onset mitochondrial diseases and normal ageing is a result of mosaic halting of mitophagy. Goljanek-Whysall et al. (2020) used the mito-QC assay to show that

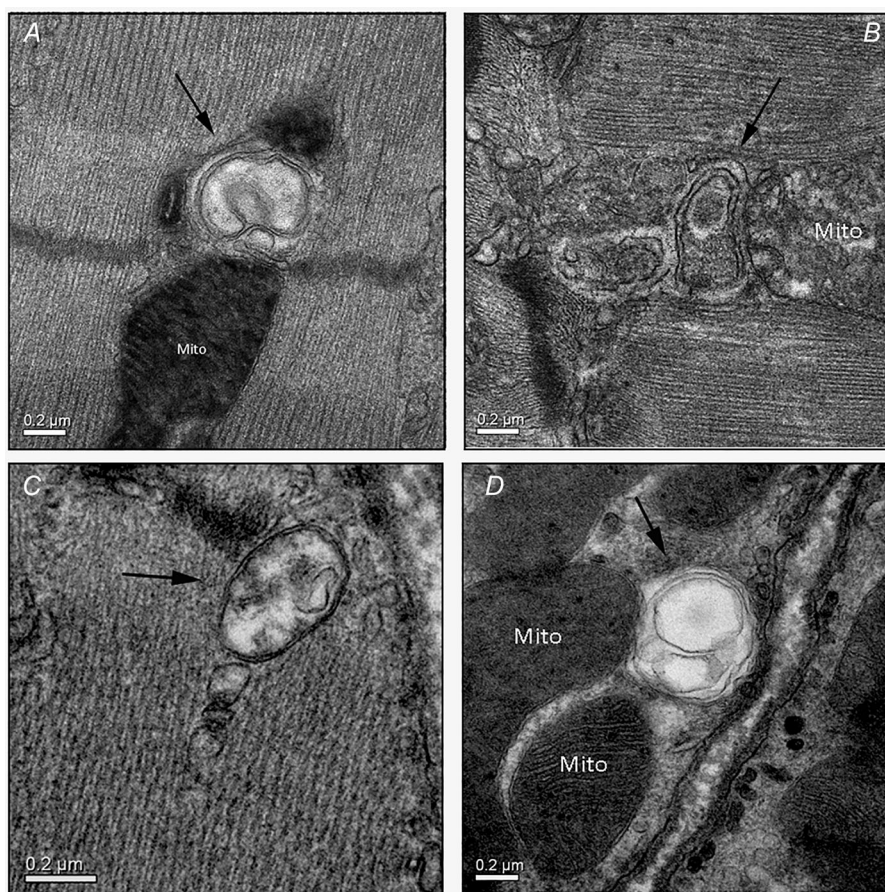


Figure 6. Autophagosome formation in response to LPS injection

Representative transmission electron microscopy of TA (A and B) and DIA (C and D) of mito-QC mice injected with LPS. Black arrows indicate autophagosomes. Mito, mitochondria.

microRNA 181 regulates muscle mitochondrial dynamics through increased mitophagy. Finally, Chernyavskij et al. (2023) reported that mitochondrial-derived oxidative stress and mitophagy activation contribute to myogenesis inhibition by tumour necrosis factor.

In the present study, we employed the mitochondrial uncoupler CCCP to confirm the ability of the mito-QC model to identify alterations in mitophagy levels within cultured muscle cells and intact muscle fibres. Our findings demonstrate that a 12 h CCCP treatment led to a notable rise in the number of mitolysosomes (normalized according to either surface area or mitochondrial content) in cultured primary myotubes derived from mito-QC mice (Fig. 1). These observations align with the findings of Allen et al. (2013) who reported a significant induction of mitophagy in CCCP-treated cultured SH-SY5Y neuroblastoma cells. Furthermore, we utilized intramuscular CCCP injection, revealing a more than six-fold increase in the number of mitolysosomes in the TA muscle (Fig. 2).

These results substantiate the applicability of the mito-QC model for discerning muscle mitophagy within both *in vitro* and *in vivo* muscle preparations.

Basal mitophagy in skeletal muscles

A significant finding in the present study is the observation that basal mitophagy in skeletal muscles is inversely correlated to muscle mitochondrial contents in normal mice. Previous studies have investigated the relationship between autophagy and muscle metabolism. For example, Montava-Garriga et al. (2020) described a positive correlation between muscle mitophagy and glycolytic activity. Likewise, Alshudukhi et al. (2018) found higher mitophagy levels in the glycolytic extensor digitorum longus muscle compared to the soleus muscle. Notably, our research group previously documented a negative correlation between basal autophagic flux and

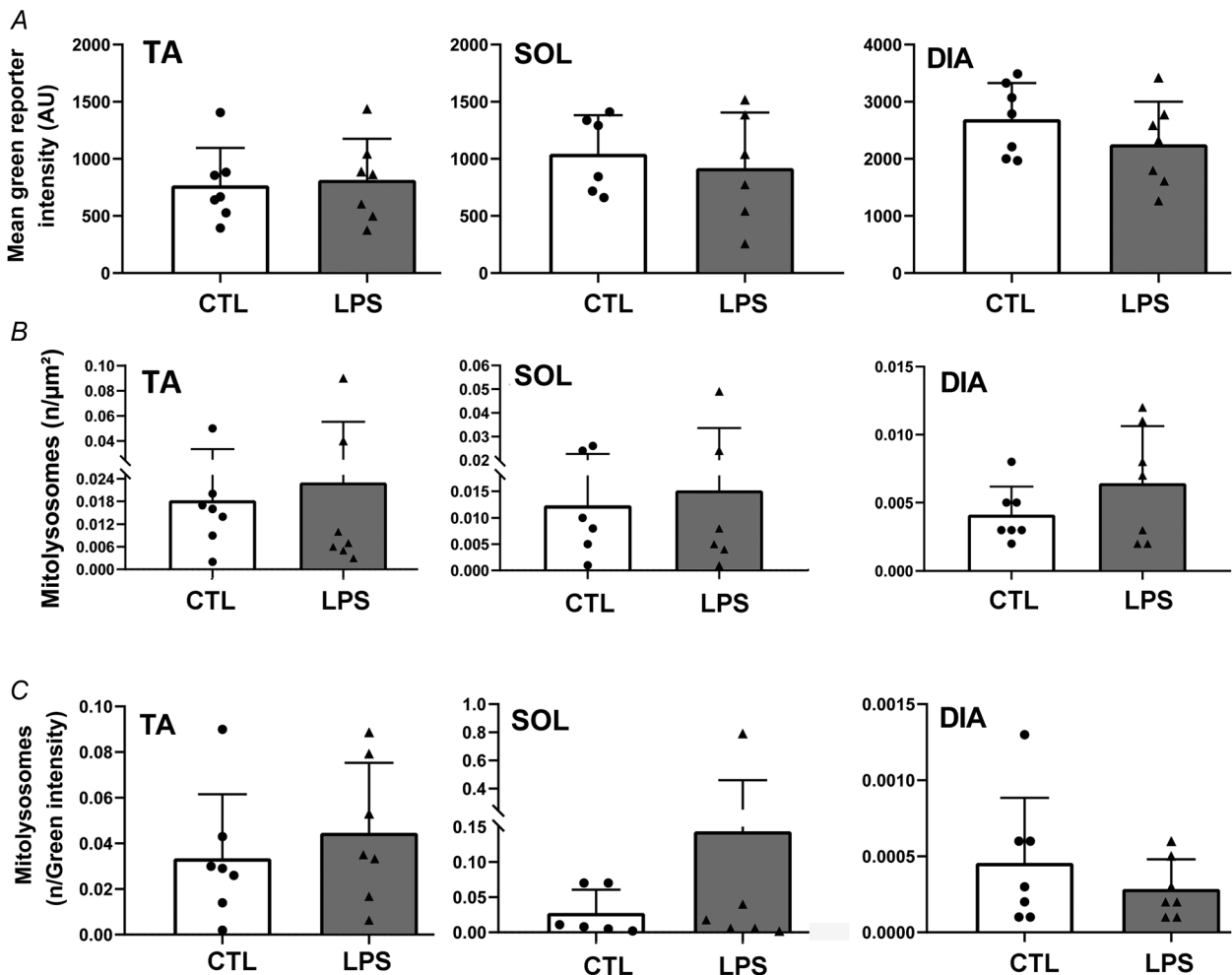


Figure 7. Impact of LPS injection on muscle mitophagy
 Mean ± SD of green reporter intensity (A), number of mitolysosomes normalized per muscle surface area (B) and mitochondrial content (C) in the TA, SOL and DIA of control and LPS-injected mito-QC mice.

muscle oxidative capacity in normal mice (Mofarrahi et al., 2013).

The mechanisms underlying the negative correlation between basal mitophagy and muscle mitochondrial contents remain unclear. Generally, mitophagy is orchestrated through two main pathways: the PINK1/Parkin-dependent and the receptor-dependent pathways. In the PINK1/Parkin-dependent mitophagy pathway, the most extensively characterized route, the loss of mitochondrial membrane potential triggers the stabilization of PINK1 protein on the outer mitochondrial membrane (OMM). Subsequently, Parkin protein is recruited, leading to the ubiquitination of several OMM proteins, including Mfn1, Mfn2, Tomm20 and VDAC. These ubiquitinated proteins facilitate the recruitment of autophagosomes, ultimately resulting in the removal of depolarized mitochondria (Narendra et al., 2010). Conversely, the receptor-mediated mitophagy pathway involves several mitophagy receptors, such as BNIP3, BNIP3L, OPTN, NDP52, FUN14 domain-containing protein 1 (FUNDC1), Bcl2 like 13 (BCL2L13),

FK506-binding protein 8 (FKBP8) and prohibitin 2 (PHB2) (Zhang et al., 2022). These receptors interact with ubiquitinated proteins on the OMM of depolarized mitochondria, as well as the LC3 protein localized to autophagosomes, leading to the elimination of depolarized mitochondria by autophagosomes (Birgisdottir Å et al., 2013).

The specific contributions of the PINK1/Parkin- and receptor-mediated pathways to muscle mitophagy remain unexplored. It is plausible that muscles characterized by lower mitochondrial contents, such as the GAS and TA, may exhibit a comparatively higher abundance of mitophagy-related proteins, potentially resulting in elevated basal mitophagy levels compared to muscles with higher mitochondrial contents. Currently, there is a scarcity of studies assessing mitophagy-related protein levels in skeletal muscles. We measured the mRNA expression of various mitophagy receptors in the GAS, TA, SOL and DIA muscles of normal mice and found no consistent correlations between mitophagy receptor expression and muscle mitochondrial contents

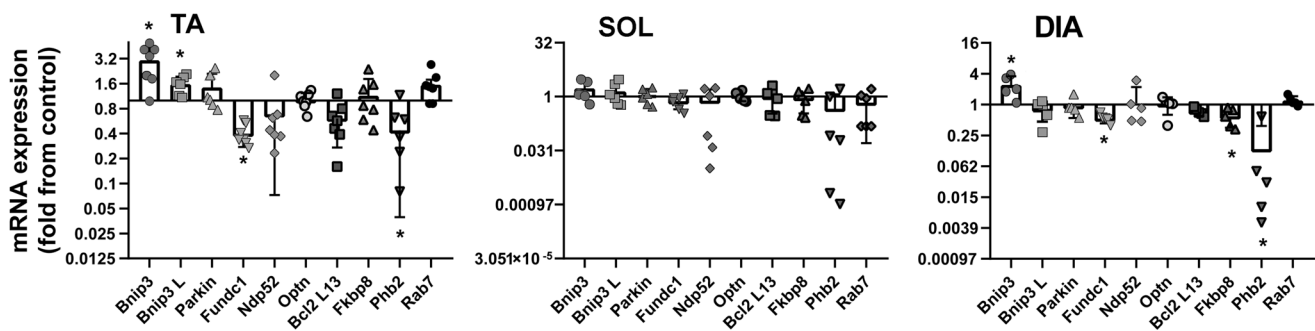


Figure 8. Impact of LPS injection on muscle mitophagy receptor expression

Mean \pm SD of mRNA expression of various mitophagy receptors in the TA ($n = 7$; CTL vs. LPS for Bnip3, Bnip3L, Fundc1 and Phb2, $P = 0.0053$; 0.0101 ; 0.0072 ; and 0.0327 , respectively), SOL ($n = 6$) and the DIA ($n = 5$; CTL vs. LPS for Bnip3, Fundc1, Fkbp8 and Phb2, $P = 0.0248$; 0.00005 ; 0.0160 ; and 0.0045 , respectively) of mito-QC mice injected with LPS. Data are expressed as fold change from values measured in control mice. Statistically significant: * $P < 0.05$ compared to control.

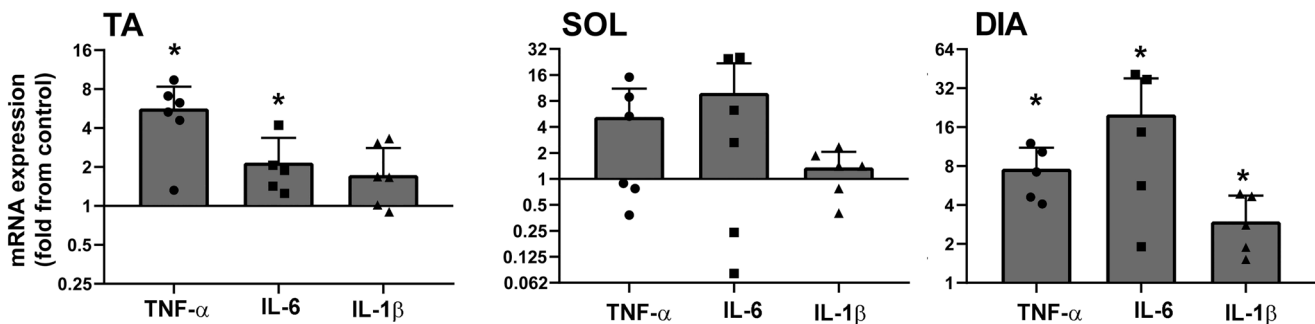


Figure 9. Impact of LPS injection on muscle-derived pro-inflammatory cytokines

Mean \pm SD of TNF- α , IL-6 and IL-1 β expression in the TA [CTL vs. LPS for TNF alpha ($n = 6$), IL-6 ($n = 5$) and IL-1beta ($n = 7$), $P = 0.0024$; 0.0457 ; and 0.1999 , respectively], SOL ($n = 6$; CTL vs. LPS for TNF alpha, IL-6 and IL-1beta, $P = 0.1143$; 0.1004 ; and 0.4885 , respectively) and the DIA ($n = 5$; CTL vs. LPS for TNF- α , IL-6 and IL-1 β , $P = 0.0032$; 0.0453 ; and 0.0364 , respectively) of mito-QC mice injected with LPS. Data are expressed as fold change from values measured in control mice. Statistically significant: * $P < 0.05$ compared to control.

(Sedraoui et al., 2024, Unpublished raw data). Another protein that may contribute to the variations in mitophagy levels among the four muscles is the UNC51-like kinase 1 (ULK1), the catalytic component of the autophagy pre-initiation complex that stimulates autophagy (Kaizuka & Mizushima, 2016; Zachari & Ganley, 2017). ULK1 has also been implicated in the induction of mitophagy (Egan et al., 2011; Murakawa et al., 2019). A recent study demonstrated that ULK1 primarily promotes mitophagy by phosphorylating BNIP3 and BNIP3L, leading to their stabilization and interaction with LC3, resulting in colocalization with Tomm20-positive mitochondria (Poole et al., 2021). In our earlier study, we observed a five-fold higher level of Ulk1 protein in the GAS and TA muscles compared to the DIA and SOL (Mofarrahi et al., 2012).

Another pertinent factor is the production of reactive oxygen species (ROS) and the levels of antioxidant enzymes in various muscles. Reports indicate that, despite glycolytic muscles having lower mitochondrial contents than oxidative muscles, the free radical leak (H_2O_2 production/ O_2 consumption) is two- to three-fold higher in the former than the latter (Anderson & Neuffer, 2006). Additionally, glycolytic muscles exhibit relatively low levels of antioxidant enzymes, rendering them more susceptible to ROS-mediated mitochondrial injury. Consequently, there may be a greater reliance on the autophagy pathway for recycling damaged mitochondria in glycolytic muscles compared to oxidative muscles.

Differences in mitochondrial morphology between glycolytic and oxidative muscles could also contribute to variations in basal mitophagy. Mitochondria in glycolytic fibres are more fragmented, making them more susceptible to mitophagy compared to their oxidative counterparts (Brown et al., 2022). Furthermore, various endogenous metabolites, including Ca^{2+} , amino acids, Fe^{2+} , NAD^+ , fatty acids and cAMP-associated metabolites, might play a role in accounting for differences in the rate of basal mitophagy between glycolytic and oxidative muscles (Zhang et al., 2022).

Impact of sepsis on muscle mitophagy

Previous research has documented that exposure to LPS elicits significant alterations in muscle mitochondrial morphology and function. For example, in C2C12 murine muscle cells, exposure to LPS for 24 h triggered an increase in mitochondrial fragmentation (Eggelbush et al., 2022). Similarly, Castro-Sepulveda et al. (2023) observed significant changes in mitochondrial morphology, including alterations in cristae density and the formation of mitochondrial nanotunnels in response to LPS exposure in human skeletal myotubes. Other reports observed functionally and morphologically abnormal

mitochondria, characterized by missing internal cristae, tightly packed matrices and the presence of dense protein aggregates in limb muscles of both septic mice and humans (Fredriksson et al., 2006; Mofarrahi et al., 2012). In a more recent study, our research group also observed the accumulation of relatively large, less round and complex mitochondria in the limb muscles of septic mice (Leduc-Gaudet et al., 2020). The accumulation of dysfunctional mitochondria in septic muscles might result from inadequate mitophagy. The present study reveals that the rate of mitophagy in limb muscles and the diaphragm in septic mice remains comparable to that detected in control muscles (Fig. 7). Four potential mechanisms may underlie this observation.

First, the lack of mitophagy induction in septic muscles could potentially stem from insufficient autophagosome formation. However, we find this scenario improbable because we observed elevated Lc3b-II protein levels and an upregulation of autophagy-related gene expression in both limb muscles and the diaphragm of septic mice (Figs 4 and 5). Moreover, multiple reports substantiate significant autophagy induction in skeletal muscles of septic mice (Mofarrahi et al., 2012; Stana et al., 2017).

Second, it is plausible that the activation of the PINK1/Parkin mitophagy pathway was not sufficient in septic muscles. It has been established that the PINK1/Parkin mitophagy pathway in the heart and kidney is triggered in response to sepsis, playing a crucial and protective role in preserving mitochondrial quality in septic tissues. Notably, sepsis-induced myocardial contractile dysfunction and kidney impairment are exacerbated in mice lacking PINK1 (Wang et al., 2021) or Parkin (Piquereau et al., 2013). However, we propose that the activation of the PINK1/Parkin pathway might not be adequate in preventing mitochondrial dysfunction in septic skeletal muscles. This interpretation is supported by our recent observation that the degree of mitochondrial injury in septic skeletal muscles was significantly diminished when Parkin protein was overexpressed using adenoassociated virus vectors (Leduc-Gaudet et al., 2020). These findings suggest that the activation or levels of the PINK1/Parkin pathway in septic muscles might be insufficient for the recycling of dysfunctional mitochondria required.

Third, it is conceivable that the contribution of the receptor-mediated pathway to overall mitophagy might be diminished in septic muscles. Despite evidence of strong upregulation of Bnip3 in septic skeletal muscles (Mofarrahi et al., 2012), the present study affirms the induction of Bnip3 expression in limb muscles and the diaphragm of septic mice (Fig. 8). However, this Bnip3 upregulation appears to be insufficient to increase mitophagy in septic skeletal muscles. Furthermore, we observed a significant downregulation in the expression of three mitophagy receptors, including Fundc1, Fkbp8

and Phb2, in septic muscles (Fig. 8). The downregulation of these receptors, such as Phb2 and Fundc1, has been recently associated with the activation of inflammatory mediators in sepsis (Chen et al., 2023). This observed downregulation of multiple mitophagy receptors may explain the lack of mitophagy induction in septic muscles.

Fourth, the absence of mitophagy induction in septic muscles might be attributed to impaired fusion of autophagosomes carrying dysfunctional mitochondria with lysosomes. The intricate process of autophagosome-lysosome fusion involves several SNARE proteins, including STX17, SNAP29, VAMP8 and VAMP7 (Tian et al., 2021). In the liver, a significant decrease in the fusion of autophagosomes with lysosomes is reported in sepsis, leading to a deficiency in the degradation of damaged mitochondria (Yin et al., 2019). It remains to be investigated whether a similar defect in autophagosome fusion with lysosomes develops in septic skeletal muscles.

A significant limitation of the present study is the absence of direct measurements of the abundance of abnormal mitochondria and the extent of mitophagy in septic skeletal muscles. It remains plausible that the level of sepsis induced by LPS injection in the present study might have been insufficient to impact mitochondrial function or morphology within skeletal muscle fibres. However, we consider this scenario improbable because numerous studies have documented substantial decreases in skeletal muscle mitochondrial function and the accumulation of abnormal mitochondria following LPS administration in mice (Aguirre et al., 2012; Mofarrahi et al., 2012; Nethery et al., 2000). Furthermore, assessments of muscle-derived pro-inflammatory cytokines indicate ongoing inflammatory responses within muscle fibres 48 h post-LPS injection (Fig. 9). Nevertheless, future investigations should focus on concurrently measuring mitochondrial morphology, injury and mitophagy in septic skeletal muscles.

The second limitation of the present study is that all experiments were conducted exclusively on male mice. Research indicates that there may be sex differences in the responses and outcomes to sepsis. Some studies report higher sepsis-related mortality in men, whereas others report higher mortality in women (Failla & Connelly 2017; Kondo et al. 2021; Sakr et al. 2013; Schroder et al. 1998). Furthermore, sex-based variations have been observed in the extent of metabolic derangement, muscle fibre atrophy and the duration of skeletal muscle weakness in sepsis patients (De Jonghe et al. 2002; Engelhardt et al. 2022). These findings underscore the need to examine how sepsis affects mitophagy and mitochondrial dysfunction in skeletal muscles of female mice.

In conclusion, our findings collectively suggest that the accumulation of abnormal mitochondria in skeletal muscles during sepsis may be the result of inadequate or

dysregulated mitophagy induction, leading to insufficient elimination of these dysfunctional mitochondria by the lysosomes. This may play a significant role in skeletal muscle dysfunction associated with these conditions, by favouring oxidative stress, loss of muscle contractility and atrophy. Future studies should delve into further assessing the impact of sepsis on specific components of the mitophagy pathway, including the contributions of individual mitophagy receptors, aiming to determine whether mitophagy can be therapeutically upregulated in these pathological conditions.

References

- Aguirre, E., López-Bernardo, E., & Cadenas, S. (2012). Functional evidence for nitric oxide production by skeletal-muscle mitochondria from lipopolysaccharide-treated mice. *Mitochondrion*, **12**(1), 126–131.
- Allen, G. F. G., Toth, R., James, J., & Ganley, I. G. (2013). Loss of iron triggers PINK1/Parkin-independent mitophagy. *European Molecular Biology Organization Reports*, **14**(12), 1127–1135.
- Alshudukhi, A. A., Zhu, J., Huang, D., Jama, A., Smith, J. D., Wang, Q. J., Esser, K. A., & Ren, H. (2018). Lipin-1 regulates Bnip3-mediated mitophagy in glycolytic muscle. *Federation of American Societies for Experimental Biology Journal*, **32**(12), 6796–6807.
- Anderson, E. J., & Neuffer, P. D. (2006). Type II skeletal myofibers possess unique properties that potentiate mitochondrial H(2)O(2) generation. *American Journal of Physiology-Cell Physiology*, **290**(3), C844–C851.
- Azuélos, I., Jung, B., Picard, M., Liang, F., Li, T., Lemaire, C., Giordano, C., Hussain, S., & Petrof, B. J. (2015). Relationship between autophagy and ventilator-induced diaphragmatic dysfunction. *Anesthesiology*, **122**(6), 1349–1361.
- Birgisdottir, Á. B., Lamark, T., & Johansen, T. (2013). The LIR motif - crucial for selective autophagy. *Journal of Cell Science*, **126**(15), 3237–3247.
- Brown, A. D., Fogarty, M. J., & Sieck, G. C. (2022). Mitochondrial morphology and function varies across diaphragm muscle fiber types. *Respiratory Physiology & Neurobiology*, **295**, 103780.
- Castro-Sepulveda, M., Tunon-Suarez, M., Rosales-Soto, G., Vargas-Foitzick, R., Deldicque, L., & Zbinden-Focsa, H. (2023). Regulation of mitochondrial morphology and cristae architecture by the TLR4 pathway in human skeletal muscle. *Frontiers in Cell Development Biology*, **11**, 121779.
- Chen, S., Ma, J., Yin, P., & Liang, F. (2023). The landscape of mitophagy in sepsis reveals PHB1 as an NLRP3 inflammasome inhibitor. *Frontiers in Immunology*, **14**, 1188482.
- Chernyavskij, D. A., Pletjushkina, O. Y., Kashtanova, A. V., Galkin, I. I., Karpukhina, A., Chernyak, B. V., Vassetzky, Y. S., & Popova, E. N. (2023). Mitochondrial oxidative stress and mitophagy activation contribute to TNF-dependent impairment of myogenesis. *Antioxidants (Basel)*, **12**(3), 602.

- De Jonghe, B., Groupe de Reflexion et 'Etdude des Neuro-mypathies en Reanimation. (2002). Paresis acquired in the intensive care unit: a prospective multicenter study. *Journal of the American Medical Association*, **288**(22), 2859–2867.
- Duan, K., Petralia, R. S., Wang, Y.a-X., & Li, Z. (2022). Analyzing autophagosomes and mitophagosomes in the mouse brain using electron microscopy. *STAR Protocol*, **3**(1), 101154.
- Egan, D. F., Shackelford, D. B., Mihaylova, M. M., Gelino, S., Kohnz, R. A., Mair, W., Vasquez, D. S., Joshi, A., Gwinn, D. M., Taylor, R., Asara, J. M., Fitzpatrick, J., Dillin, A., Viollet, B., Kundu, M., Hansen, M., & Shaw, R. J. (2011). Phosphorylation of ULK1 (hATG1) by AMP-activated protein kinase connects energy sensing to mitophagy. *Science*, **331**(6016), 456–461.
- Eggelbusch, M., Shi, A., Broeksma, B. C., Vázquez-Cruz, M., Soares, M. N., De Wit, G. M. J., Everts, B., Jaspers, R. T., & Wüst, R. C. I. (2022). The NLRP3 inflammasome contributes to inflammation-induced morphological and metabolic alterations in skeletal muscle. *Journal of Cachexia Sarco Muscle*, **13**(6), 3048–3061.
- Engelhardt, L. J.o., Grunow, J. J., Wollersheim, T., Carbon, N. M., Balzer, F., Spranger, J., & Weber-Carstens, S. (2022). Sex-specific aspects of skeletal muscle metabolism in the clinical context of intensive care unit-acquired weakness. *Journal of Clinical Medicine*, **11**(3), 846.
- Failla, K. R., & Connelly, C. D. (2017). Systematic review of gender differences in sepsis management and outcomes. *Journal of Nursing Scholarship*, **49**(3), 312–324.
- Fan, E., Cheek, F., Chlan, L., Gosselink, R., Hart, N., Herridge, M. S., Hopkins, R. O., Hough, C. L., Kress, J. P., Latronico, N., Moss, M., Needham, D. M., Rich, M. M., Stevens, R. D., Wilson, K. C., Winkelman, C., Zochodne, D. W., & Ali, N. A. (2014). An official American Thoracic Society Clinical Practice guideline: The diagnosis of intensive care unit-acquired weakness in adults. *American Journal of Respiratory and Critical Care Medicine*, **190**(12), 1437–1446.
- Fredriksson, K., Hammarqvist, F., Strigård, K., Hulténby, K., Ljungqvist, O., Wernerman, J., & Rooyackers, O. (2006). Derangements in mitochondrial metabolism in intercostal and leg muscle of critically ill patients with sepsis-induced multiple organ failure. *American Journal of Physiology-Endocrinology and Metabolism*, **291**(5), E1044–E1050.
- Goljanek-Whysall, K., Soriano-Arroquia, A., McCormick, R., Chinda, C., & McDonagh, B. (2020). miR-181a regulates p62/SQSTM1, parkin, and protein DJ-1 promoting mitochondrial dynamics in skeletal muscle aging. *Aging Cell*, **19**(4), e13140.
- Kaizuka, T., & Mizushima, N. (2016). Atg13 is essential for autophagy and cardiac development in mice. *Molecular and Cellular Biology*, **36**(4), 585–595.
- Klionsky, D. J. (2008). Autophagy revisited: A conversation with Christian de Duve. *Autophagy*, **4**(6), 740–743.
- Kondo, Y., Miyazato, A., Okamoto, K., & Tanaka, H. (2021). Impact of sex differences on mortality in patients with severe sepsis after trauma: A nationwide cohort study. *Frontiers in Immunology*, **12**, 678156.
- Leduc-Gaudet, J. P., Hussain, S. N. A., Barreiro, E., & Gouspillou, G. (2021). Mitochondrial dynamics and mitophagy in skeletal muscle health and aging. *International Journal of Molecular Sciences*, **22**(15), 8179.
- Leduc-Gaudet, J.-P., Mayaki, D., Reynaud, O., Broering, F. E., Chaffer, T. J., Hussain, S. N. A., & Gouspillou, G. (2020). Parkin overexpression attenuates sepsis-induced muscle wasting. *Cells*, **9**(6), 1454.
- McWilliams, T. G., & Ganley, I. G. (2019). Investigating mitophagy and mitochondrial morphology in vivo using mito-QC: A comprehensive guide. *Methods in Molecular Biology*, **1880**, 621–642.
- McWilliams, T. G., Prescott, A. R., Allen, G. F. G., Tamjar, J., Munson, M. J., Thomson, C., Muqit, M. M. K., & Ganley, I. G. (2016). mito-QC illuminates mitophagy and mitochondrial architecture in vivo. *Journal of Cell Biology*, **214**(3), 333–345.
- Mito, T., Vincent, A. E., Faitg, J., Taylor, R. W., Khan, N. A., McWilliams, T. G., & Suomalainen, A. (2022). Mosaic dysfunction of mitophagy in mitochondrial muscle disease. *Cell Metabolism*, **34**(2), 197–208. e5.
- Mofarrahi, M., Guo, Y., Haspel, J. A., Choi, A. M.k, Davis, E. C., Gouspillou, G., Hepple, R. T., Godin, R., Burelle, Y., & Hussain, S. N. A. (2013). Autophagic flux and oxidative capacity of skeletal muscles during acute starvation. *Autophagy*, **9**(10), 1604–1620.
- Mofarrahi, M., Sigala, I., Guo, Y., Godin, R., Davis, E. C., Petrof, B., Sandri, M., Burelle, Y., & Hussain, S. N. A. (2012). Autophagy and skeletal muscles in sepsis. *PLoS ONE*, **7**(10), e47265.
- Montava-Garriga, L., Singh, F., Ball, G., & Ganley, I. G. (2020). Semi-automated quantitation of mitophagy in cells and tissues. *Mechanisms of Ageing and Development*, **185**, 111196.
- Murakawa, T., Okamoto, K., Omiya, S., Taneike, M., Yamaguchi, O., & Otsu, K. (2019). A mammalian mitophagy receptor, Bcl2-L-13, recruits the ULK1 complex to induce mitophagy. *Cell Reports*, **26**(2), 338–345. e6.e336.
- Narendra, D. P., Jin, S. M., Tanaka, A., Suen, D.-F., Gautier, C. A., Shen, J., Cookson, M. R., & Youle, R. J. (2010). PINK1 is selectively stabilized on impaired mitochondria to activate Parkin. *PLoS Biology*, **8**(1), e1000298.
- Nethery, D., Callahan, L. A., Stofan, D., Mattera, R., Dimarco, A., & Supinski, G. (2000). PLA2 dependence of diaphragm mitochondrial formation of reactive oxygen species. *Journal of Applied Physiology*, **89**(1), 72–80.
- Petrof, B. J. (2018). Diaphragm weakness in the critically ill: Basic mechanisms reveal therapeutic opportunities. *Chest*, **154**(6), 1395–1403.
- Picard, M., White, K., & Turnbull, D. M. (2013). Mitochondrial morphology, topology, and membrane interactions in skeletal muscle: A quantitative three-dimensional electron microscopy study. *Journal of Applied Physiology* (1985), **114**(2), 161–171.
- Piquereau, J., Godin, R., Deschênes, S., Bessi, V. L., Mofarrahi, M., Hussain, S. N. A., & Burelle, Y. (2013). Protective role of PARK2/Parkin in sepsis-induced cardiac contractile and mitochondrial dysfunction. *Autophagy*, **9**(11), 1837–1851.

- Poole, L. P., Bock-Hughes, A., Berardi, D. E., & Macleod, K. F. (2021). ULK1 promotes mitophagy via phosphorylation and stabilization of BNIP3. *Scientific Reports*, **11**(1), 20526.
- Sakr, Y., Elia, C., Mascia, L., Barberis, B., Cardellino, S., Livigni, S., Fiore, G., Filippini, C., & Ranieri, V. (2013). The influence of gender on the epidemiology of and outcome from severe sepsis. *Critical Care*, **17**(2), R50.
- Schröder, J. (1998). Gender differences in human sepsis. *Archives of Surgery*, **133**(11), 1200–1205.
- Sedraoui, S., Mayaki, D., Petrof, B. J., & Hussain, S. N. A. (2024). Correlation between mitophagy receptor expression and mitochondrial contents in skeletal muscles of mice. [Unpublished raw data].
- Stana, F., Vujovic, M., Mayaki, D., Leduc-Gaudet, J.-P., Leblanc, P., Huck, L., & Hussain, S. N. A. (2017). Differential regulation of the autophagy and proteasome pathways in skeletal muscles in sepsis. *Critical Care Medicine*, **45**(9), e971–e979.
- Tian, X., Teng, J., & Chen, J. (2021). New insights regarding SNARE proteins in autophagosome-lysosome fusion. *Autophagy*, **17**(10), 2680–2688.
- Wang, Y., Zhu, J., Liu, Z., Shu, S., Fu, Y., Liu, Y., Cai, J., Tang, C., Liu, Y., Yin, X., & Dong, Z. (2021). The PINK1/PARK2/optineurin pathway of mitophagy is activated for protection in septic acute kidney injury. *Redox Biology*, **38**, 101767.
- Yin, X., Xin, H., Mao, S., Wu, G., & Guo, L. (2019). The role of autophagy in sepsis: Protection and injury to organs. *Frontiers in Physiology*, **10**, 1071.
- Zachari, M., & Ganley, I. G. (2017). The mammalian ULK1 complex and autophagy initiation. *Essays in Biochemistry*, **61**, 585–596.
- Zhang, T., Liu, Q., Gao, W., Sehgal, S. A., & Wu, H. (2022). The multifaceted regulation of mitophagy by endogenous metabolites. *Autophagy*, **18**(6), 1216–1239.

Additional information

Data availability statement

All data supporting the results of the present study are included within the published paper.

Competing interests

The authors declare that they have no competing interests.

Author contributions

S.S., S.H. and B.J.P. designed and conceived the study. S.S., J.-P.L.-G., D.M., A.M. and L.H. collected and analysed the data. S.S., S.H. and B.J.P. analysed the data and interpreted the results. S.S. and S.H. wrote the first draft of the manuscript. S.H., B.J.P. and G.G. supervised the research, contributed to data analysis and interpretation, and wrote the final version of the manuscript with S.S. S.H. and B.J.P. were responsible for funding acquisition. All authors have read and approved the final version of the manuscript submitted for publication.

Funding

This study is supported by grants from the Natural Sciences and Engineering Council of Canada and Canadian Institutes of Health Research. S. Sedraoui was supported by post-doctoral fellowship from the Meakins-Christie Laboratories, McGill University.

Acknowledgements

We are grateful to I. Ganley (University of Dundee) for providing the mito-QC mice and aiding with measurements of mitolysosomes in the present study.

Keywords

autophagy, mitochondria, mitophagy, mito-QC, sepsis, skeletal muscles

Supporting information

Additional supporting information can be found online in the Supporting Information section at the end of the HTML view of the article. Supporting information files available:

Peer Review History